Bulletin of the Seismological Society of America, Vol. 103, No. 1, pp. 19–32, February 2013, doi: 10.1785/0120120008

A Nonlinear Site-Amplification Model for the Next Pan-European Ground-Motion Prediction Equations

by M. Abdullah Sandıkkaya,* Sinan Akkar, and Pierre-Yves Bard

Abstract A site-amplification model for shallow crustal regions that considers both linear and nonlinear soil effects is proposed. The original functional form of the model was developed by Walling *et al.* (2008) (WAS08) using stochastic simulations and site-response analysis. The major difference between the proposed model and WAS08 is that our site-amplification expression is entirely based on empirical data. To comply with this objective, a database with the most recent V_{S30} information from the pan-European region has been compiled. This feature of the model encourages its use for the future ground-motion prediction equations (GMPEs) that will be devised particularly for this region. Worldwide accelerograms are also considered to have a better representation of the soil behavior under strong-motion excitations. As an auxiliary tool a GMPE for reference-rock sites is also developed to calculate the site-amplification factors. The coefficients of the site-amplification model as well as the reference-rock model are computed by applying the random-effects regression technique proposed by Abrahamson and Youngs (1992). Preliminary results of this article suggest a more comprehensive study for the revision of site factors in Eurocode 8 (European Committee for Standardization [CEN], 2004).

Online Material: Tables of database statistics, regression coefficients, and standard deviations.

Introduction

The recent trend in ground-motion prediction equations (GMPEs) is to represent the soil effects by a site-amplification model that mimics the soil behavior through functional forms that are either based on stochastic simulations or empirical data. The site conditions are generally described by the time-based average of the shear-wave velocity profile in the upper 30 m of soil (V_{S30}), but some models also consider complementary parameters to this proxy to fully capture the genuine soil behavior under various circumstances (e.g., $Z1.0$ and $Z2.5$ to describe the soil response of deep alluvial deposits). Although the ongoing efforts to elaborate such additional complementary parameters are promising (e.g., Thompson *et al.*, 2011), V_{S30} still preserves its significance as an estimator to describe the overall site effect on the ground-motion estimation.

The conventional method for implementing site effects in ground-motion prediction models is to use site-amplification factors that are obtained by normalizing a chosen ground-motion intensity measure at a soil site with its counterpart measured at a nearby rock site (Borcherdt, 1970). The most important drawback of this approach is the lack of nearby rock sites while characterizing the site amplification for that specific event. One way of overcoming this drawback is to calibrate the ground motions at the site of interest by a geometrical spreading factor without modifying the particular site features to imitate their behavior at reference-rock sites. This way the analyst can employ the conventional procedure by normalizing the amplitudes of calibrated ground motions with that of the reference-rock site. Borcherdt (1994, 2002a,b) and Dobry *et al.* (2000) utilized this approach for the Loma Prieta and Northridge earthquakes and obtained the site factors that formed the basis of the U.S. National Earthquake Hazard Risk Reduction Program (NEHRP) site-amplification factors (Building Seismic Safety Council [BSSC], 2009a,b). Although this procedure increases the number of usable recordings for site-amplification studies, the likely regional dependency of the geometrical spreading function may become critical for reliable modification of the recordings, which are collected from various regions of different crustal features.

Another efficient way of estimating the site effects on ground-motion amplitudes is to use stochastic methods (e.g., Boore, 2005) for simulating different site conditions under

*Also at ISTerre (Institut des Sciences de la Terre), Universite de Grenoble, 38041 Grenoble Cedex 9, France.

different earthquake scenarios. Boore and Joyner (1997) presented the groundbreaking and pioneer study in this field that proposes site-amplification factors at different spectral frequencies using the quarter-wavelength theory and stochastic simulations representing generic site classes. More recent studies (e.g., Ni *et al.*, 2000; Walling *et al.*, 2008; WAS08) generate stochastic reference-rock motions and convolve the soil motion associated with different features via site-response analysis to modify the simulated rock motion. This way they derive site models for different soil conditions by modeling the site amplification between rock and soil motion through regressions on various functional forms. Following a similar concept, Sokolov (1997, 2000) first simulated the reference-rock motions at specific sites and then normalized the actual ground motions recorded at these sites with the generated reference-rock simulations to derive his site-amplification factors. As in the case of recorded ground motions the level of accuracy in stochastic simulations depends on the reliability of source information as well as the site features described by geophysical and geotechnical parameters. Nevertheless, they contain very useful information for describing the functional form of the site model provided that they are based on the right physics for the background nonlinear model and the right order of magnitude for the corresponding soil nonlinear parameters.

An alternative to the above approaches is the utilization of existing empirical ground-motion predictive models for describing the reference-rock conditions to compute site-amplification factors by normalizing the observed ground motions with the estimated reference-rock motions. Studies conducted by Field (2000), Lee and Anderson (2000), Steidl (2000), Stewart *et al.* (2003) and Choi and Stewart (2005; CS05) consider this methodology either to observe the variation of site amplifications for different soil conditions or to derive site models for their use in GMPEs. Instead of employing the existing GMPEs to represent the reference-rock motion, some studies derive specific predictive models to mimic different site conditions, including the reference rock, to compute the site factors through a similar normalization scheme as described above (e.g., Crouse and McGuire, 1996; Rodriguez-Marek *et al.*, 2001).

The main objective of this article is to propose an empirical site-amplification model to be used in GMPEs for shallow active crustal regions. The proposed model can capture the nonlinear soil effects as a function of V_{S30} for different input rock-motion levels. The strong-motion database of this article is based on a subset of an extensive strong-motion databank that has been compiled in the framework of the project entitled Seismic Hazard HARmonization in Europe (SHARE). The selected database includes recordings from Europe and surrounding regions (Greek, Italian, and Turkish strong-motion recordings) with measured shear-wave (*S*-wave) velocity information. The database also contains strong-motion data collected from Taiwan, Japan, and California with measured V_{S30} values for a broader coverage of soil behavior. A relatively large amount of pan-European data can make the model useful for future pan-European GMPEs. The proposed site-amplification function employs a reference-rock model that is derived from a subset of the ground-motion database. This step is different in most of the similar studies, because they either import the reference-rock model from another research or use theoretical simulations to describe rock motion. The site amplifications computed by normalizing the observed data with the estimations obtained from the reference-rock model are regressed by modifying the WAS08 site function that is derived from the stochastic simulations.

The paper first discusses the previous site models with special emphasis on recent GMPEs developed in the Next Generation Attenuation (NGA) project (Power *et al.*, 2008). Important observations from the NGA GMPEs constitute one of the major motivations of this article and are used in the development of the nonlinear soil model presented here. The strong-motion database used in the derivation of the nonlinear site model and comparisons of the proposed model with the existing ones are the other important topics in this article. A short discussion on the NEHRP (BSSC, 2009a) and Eurocode 8 (European Committee for Standardization [CEN], 2004) site factors is also included under the findings of the article.

Site-Amplification Functions with Emphasis on the NGA Models

The integration of soil effects in GMPEs evolved progressively. In early GMPEs, the site effects were addressed by defining two broad site classifications (soil and rock). As a recent example, Sadigh *et al.* (1997) determined the site coefficients by employing separate regressions on rock and soil datasets. Other ground-motion models accounted for the site influence by considering more detailed soil categories that are based on certain V_{S30} intervals. In such GMPEs (e.g., Akkar and Bommer, 2010), the same source and path models were used and the differences arising from site effects are represented by different soil coefficients for each site category. Boore *et al.* (1997; BJF97), proposed a more complicated site model that is a continuous function of V_{S30} (equation 1). In this model, the logarithm of the site amplification (ln[Amp]) is proportional to the logarithm of V_{S30} normalized by a period-dependent reference velocity, $V_{\mathrm{LIN}}(T)$. The period-dependent coefficients $a(T)$ and $V_{\mathrm{LIN}}(T)$ are computed from regression analysis.

$$\ln(\mathrm{Amp}) = a(T)\ln[V_{S30}/V_{\mathrm{LIN}}(T)]. \qquad (1)$$

The site model proposed by BJF97, as well as the others described in the previous paragraph, do not include nonlinear soil behavior. To the best of our knowledge the Abrahamson and Silva (1997; AS97) site function is the first model that considers nonlinear soil amplification. This model classifies sites as rock and soil and applies a correction to

the ground-motion amplitudes of soil sites to consider the nonlinear site effects as a function of input rock-motion level (PGA_{rock}). The AS97 site function is given in equation (2) in which the period-dependent coefficients, $a(T)$ and $b(T)$, are determined from regression analysis and the period-independent coefficient, c, is constrained to $0.03g$ for the entire period range.

$$\ln(\text{Amp}) = a(T) + b(T)\ln(\text{PGA}_{\text{rock}} + c). \qquad (2)$$

CS05, in a way, combined equations (1) and (2) to obtain a site model that represents both linear and nonlinear site amplification. To this end, they proposed linear and nonlinear site terms that are functions of period and V_{S30} (equation 3). This functional form modifies the PGA_{rock}-dependent logarithmic expression to account for the overall nonlinear soil response as follows:

$$\ln(\text{Amp}) = a(T)\ln[V_{S30}/V_{\text{LIN}}(T)] + b(V_{S30}, T)\ln(PGA_{\text{rock}}/0.1). \qquad (3)$$

The amplification factors in CS05 are computed by normalizing the observed acceleration-spectrum ordinates with the corresponding estimations obtained from the reference-rock model of AS97. CS05 assumes the reference rock V_{S30} as 760 m/s, although the reference-rock definition of AS97 corresponds to an average V_{S30} value of 550 m/s (Walling *et al.*, 2008). CS05 accommodates this discrepancy by suggesting a modification in their site amplification.

Boore and Atkinson (2008) (BA08), one of the model developers in the NGA project, integrated the CS05 site model to their GMPE with some adjustments. The period-dependent V_{LIN} parameter in CS05 is a fixed reference V_{S30} value in BA08 that is called $V_{\text{REF}}(V_{\text{REF}} = 760$ m/s). V_{REF} also describes the reference-rock site in BA08. The overall contribution of soil nonlinearity in BA08 is formulated for three levels of input reference-rock motion (i.e., $PGA_{rock} \leq 0.03g$; $0.03g < PGA_{rock} \leq 0.09g$; $PGA_{rock} > 0.09g$). Furthermore, BA08 modified the b (V_{S30}, T) term with a piecewise linear function (referred to as b_{nl} in their terminology). Figure 1a shows the peak ground acceleration (PGA) site amplifications of CS05 and BA08 at different PGA_{rock} levels. Figure 1b compares the behavior of b (V_{S30}, T) with b_{nl} for $T = 0.0$ s. As inferred from Figure 1a the CS05 model results in a kink in site amplification in the vicinity of $V_{S30} = 520$ m/s due to the discontinuity in the b (V_{S30}, T) term at this V_{S30} value (Fig. 1b). The BA08 model removes this behavior by introducing a smooth transition in b_{nl} between 300 m/s $\leq V_{S30} \leq$ 760 m/s (Fig. 1b). However, this smooth transition imposes lower nonlinear soil behavior with respect to CS05 for 300 m/s $\leq V_{S30} \leq$ 520 m/s. On the contrary, the linear trend in b_{nl} between 180 m/s $< V_{S30} <$ 300 m/s yields slightly higher soil nonlinearity with respect to CS05. Figure 1a also shows that BA08 results in higher amplification levels with respect to those of CS05 when V_{S30} attains larger values (i.e., $V_{S30} > 300$ m/s). This behavior can be attributed to the modifications to the V_{LIN} parameter by BA08, because linear site behavior generally governs for $V_{S30} > 300$ m/s as will be discussed in the following paragraphs. This observation suggests that the BA08 model would estimate larger site amplifications for linear soil behavior. In fact the use of period-independent V_{REF} in BA08 seems to shift the site amplifications towards higher values for the entire V_{S30} band at all rock PGA levels except for those of low V_{S30} sites subjected to low ground-motion amplitudes (mimicked by $PGA_{rock} \leq 0.03g$ in Fig. 1a). For very low ground-motion amplitudes the BA08 model prevents the increase in soil nonlinearity at softer sites by imposing a constant nonlinear amplification at the lowest range of input rock motion (i.e., $PGA_{rock} \leq 0.03g$). This fact is not accounted for by CS05. The lower bound of V_{S30} for CS05 and BA08 is 180 m/s. However, the plots on Figure 1 extend V_{S30} towards much

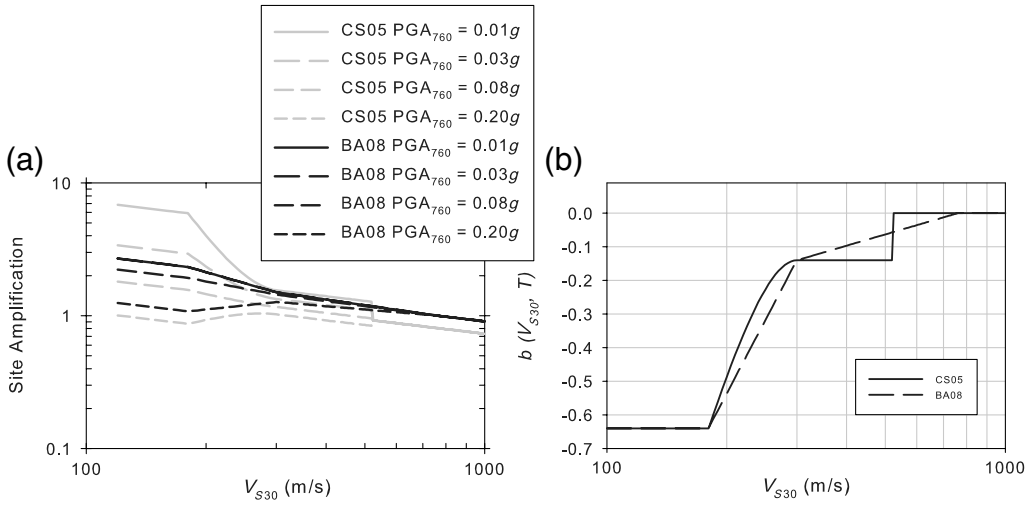

Figure 1 (a) Comparisons between the amplification factors derived from CS05 and BA08 for PGA. Each line represents different levels of input rock motion. (b) Comparison of the nonlinear coefficients for $T = 0.0$ s proposed by CS05 and BA08.

smaller values to show the behavior of these models if they are used for addressing soil amplification at low-velocity sites.

The site model proposed by Chiou and Youngs (2008; CY08) was also developed within the framework of NGA project and is similar to CS05. CY08 derived their functional form by interpreting the studies of BJF97 and AS97. The reference velocity that is considered as 760 m/s in BA08 is 1130 m/s in CY08 by assuming that no major soil nonlinearity can take place beyond this velocity level. The site amplification is set to unity for V_{S30} values greater than 1130 m/s. Contrary to BA08, which uses the site coefficients of CS05, CY08 determined the site coefficients by regressing on their own database that led to better representation of the data trend. Another important difference of CY08 with respect to other models is that the nonlinear site-response term is expressed by reference-rock spectral accelerations (instead of reference-rock PGA) at the period of interest. This feature, according to our understanding, makes this model more complicated in terms of its implementation.

The WAS08 site model that was also developed during the course of the NGA project generated stochastic simulations for a single scenario event to obtain rock motions at $V_{S30} = 1100$ m/s. They performed site-response analysis to obtain the soil motions at certain V_{S30} values. In site-response analysis, four specific modulus and damping degradation curves were used to mimic different site conditions (i.e., Imperial Valley, Bay Mud, Peninsular range, and EPRI models). The first and second degradation curves were used when V_{S30} attains values less than 270 m/s. The third and fourth curves represent the cases for $V_{S30} \geq 270$ m/s. The site amplification was calculated by dividing the convoluted soil motions by the simulated reference-rock motions. These amplification factors were then utilized to derive the site model (equation 4) as two piecewise functions. The WAS08 model assumes linear soil response (a) when PGA_{1100} goes to zero and (b) when $V_{S30} \geq V_{\mathrm{LIN}}$. WAS08 considers PGA_{1100} as the main controlling parameter in soil nonlinearity for all spectral periods. The coefficients $a(T)$, $b(T)$, c, and n are the regression coefficients. The parameter d implicitly relates the linear transition between $V_{\mathrm{LIN}}(T)$ and the reference-rock site shear-wave velocity that is taken as 1100 m/s.

damping degradation curves. The major difference between the AS08 and CB08 models is the linear site term, because they used different subsets of the NGA database. As these models have the same origin for site response, the results obtained from AS08 are presented in this article. The site-amplification factors of AS08 are lower than unity at $V_{S30} = 1100$ m/s. The reason behind this behavior is that AS08 does not consider the d term proposed in WAS08. As a matter of fact the d term is compensated by other regression coefficients (e.g., source and path coefficients) in the ground-motion prediction model of AS08. Because one of the aims of this article is the evaluation of different site models, this parameter is included in the original AS08 in order to observe an amplification ratio of unity at $V_{S30} = 1100$ m/s. AS08 also includes another period-dependent V_{S30} parameter, V_{CON}, above which the site term becomes constant. Consequently, for $V_{S30} < V_{\mathrm{LIN}}$, the amplification is a function of PGA_{1100} and V_{S30}. For V_{S30} values between V_{LIN} and V_{CON}, the amplification depends only on V_{S30} (i.e., only linear amplification). For $V_{S30} > V_{\mathrm{CON}}$ a constant amplification is imposed by this model whatever the PGA_{1100} and V_{S30} values.

Figure 2 shows the site-amplification factors computed from BA08. (The other site models discussed in this section show fairly similar trends to those of BA08 and are not shown on this figure.) The soil nonlinearity is dominant for sites with $V_{S30} < 300$ m/s in BA08. The contribution of soil nonlinearity to site amplification decreases with increasing period when V_{S30} values are greater than 300 m/s. The influence of soil nonlinearity seems to vanish completely beyond $T = 1.0$ s and no nonlinear site effect is considered for $V_{S30} > 760$ m/s (V_{S30} for reference rock). For sites, which are located on very soft soil deposits (i.e., $V_{S30} <$ 180 m/s), the amplification trend changes and starts to increase with increasing $\mathrm{PGA}_{\mathrm{rock}}$, which is due to the use of constant nonlinear coefficient in this range. The middle column panels in Figure 2 indicate that the amplification becomes independent of V_{S30} at a certain value of $\mathrm{PGA}_{\mathrm{rock}}$. This input rock-motion level is called hinging PGA in this article and is a function of period. For PGA_{760} values that are lower than the hinging PGA, the linear site term dominates and softer sites show higher amplification. Beyond

$$\ln(\mathrm{Amp}) = \begin{cases} a(T)\ln[V_{S30}/V_{\mathrm{LIN}}(T)] - b(T)\ln(\mathrm{PGA}_{1100}+c) + b(T)\ln\{\mathrm{PGA}_{1100} + c[V_{S30}/V_{\mathrm{LIN}}(T)^n]\} + d & \text{for } V_{S30} < V_{\mathrm{LIN}}(T) \\ [a(T)+b(T)n]\ln[V_{S30}/V_{\mathrm{LIN}}(T)] + d & \text{for } V_{S30} \geq V_{\mathrm{LIN}}(T) \end{cases} \quad (4)$$

The WAS08 nonlinear site model was implemented in the Campbell and Bozorgnia (2008), and Abrahamson and Silva (2008; CB08 and AS08, respectively) GMPEs. In their site models, AS08 and CB08 used the nonlinear soil coefficients derived from the Peninsular range shear modulus and

the hinging PGA the contribution of nonlinear term increases for soft sites with low V_{S30} values. As the stiffness of the site increases, the hinging PGA shifts to a larger value. This observation indicates that for stiffer sites the BA08 model does not expect nonlinear soil behavior except for very

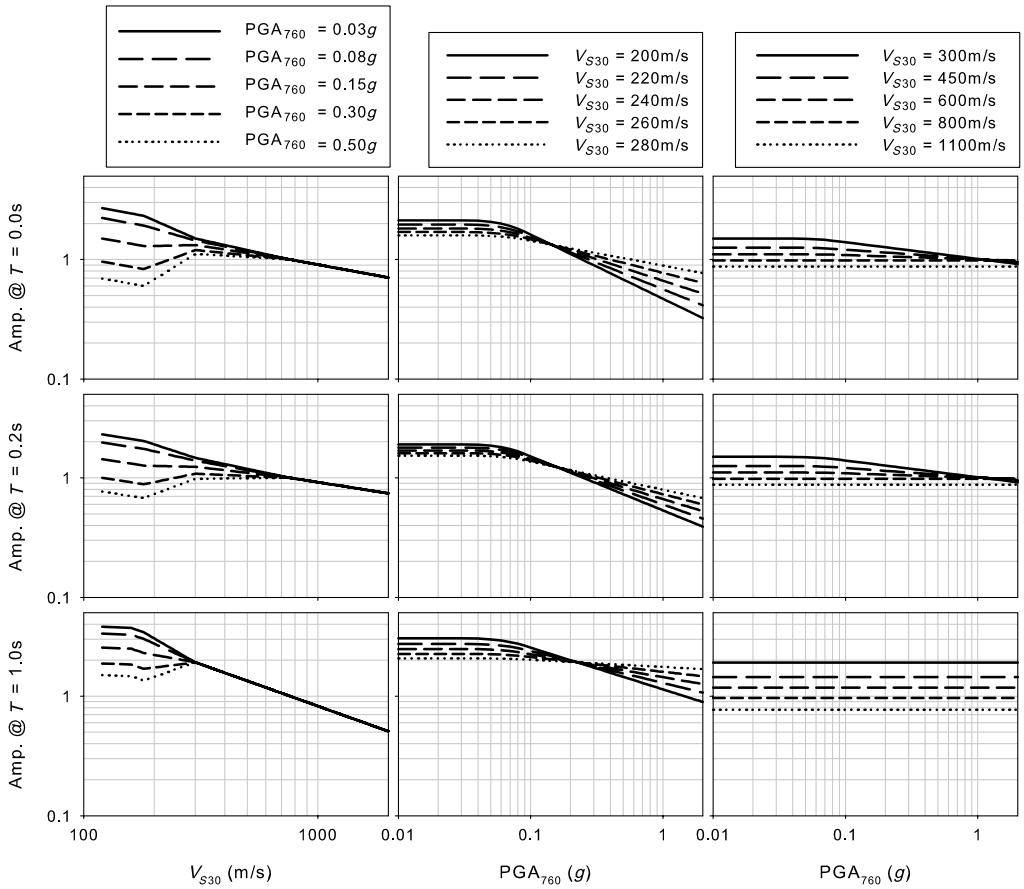

Figure 2 Site amplifications proposed by BA08 for $T = 0.0$ s, 0.2 s, and 1.0 s. The left column shows the variation of the site amplification with respect to V_{S30} for different levels of PGA_{rock}. (V_{S30} for reference rock is 760 m/s in BA08. This is emphasized by designating PGA_{rock} as PGA_{760} in the legends.) The middle and right columns show the variation of the site amplifications as a function of PGA_{rock} (PGA_{rock} is designated as PGA_{760} in x-axis labels) for different V_{S30} values. V_{S30} values range between 200 and 280 m/s in the middle column plots whereas they change from 300 to 1100 m/s in the right column plots.

strong ground motions associated with high PGA_{rock}. The hinging PGA shifts towards larger values with increasing period for $V_{S30} < 300$ m/s. The same trend is also observed for 300 m/s $< V_{S30} <$ 760 m/s at higher levels of input rock motion but in this case the amplitude of hinging PGA decreases with increasing period and vanishes after $T > 1.0$ s. This observation suggests that the BA08 model barely expects nonlinear soil behavior (i.e., PGA_{rock} values larger than hinging PGA) for stiff sites.

We note that discrepancies in the reference velocity definitions of CS05 and BA08 with respect to AS97, which can be considered as the basis of these two site models as well as the verification of single-event-based simulations used in the AS08 site function that may fail to describe the event uncertainty in soil behavior, are among the major reasons behind the derivation of the site model presented here. The other motivation of this article is the recently updated site information of the pan-European accelerograms. To this end, the proposed model can be considered as a good candidate for future pan-European GMPEs. Our strong-motion database and particular features of the proposed model are discussed in the rest of the article.

Strong-Motion Database

The strong-motion database used in this article is extracted from a comprehensive ground-motion databank, which has been compiled within the framework of the SHARE project (hereinafter SHARE SM databank). The SHARE SM databank consists of shallow active crustal accelerograms gathered from the national and global databases that are listed in Table 1 with relevant references. Details about the compilation of SHARE SM databank can be found in Yenier *et al.* (2010) that is also posted on the following: http://www.share-eu.org/sites/default/files/D4%201_SHARE.pdf (last accessed April 2012). Only recordings of measured S-wave velocities (V_S) have been selected for the present article. This decision led to a database of 5530 three-component accelerograms from 414 events recorded at 1616 sites. The moment magnitude (M_w) range of the database is $4 \leq M_w \leq 7.9$. We did not include small-magnitude events ($M_w < 4$), because the metadata parameters of small-magnitude events are generally unreliable in terms of epicenter coordinates, magnitude and depth information. The source-to-site distances of the selected recordings are $R_{JB} \leq 200$ km for which R_{JB} is the

Table 1
Strong-Motion Datasets Gathered in the SHARE SM Databank

Dataset	Number of Events	Number of Recordings	Reference
European Strong Motion Database (ESMD)	45	214	Ambraseys, Douglas, *et al.* (2004)
Internet Site for European Strong-motion Data (ISESD)	675	2046	Ambraseys, Smit, *et al.* (2004)
ITalian ACcelerometric Archive database (ITACA)	199	1165	Luzi *et al.* (2008)
K-NET database	27	987	National Research Institute for Earth Science and Disaster Prevention*
KiK-Net database	596	4704	National Research Institute for Earth Science and Disaster Prevention†
Next Generation Attenuation database (NGA)	152	3403	Chiou *et al.* (2008)
Turkish National Strong-Motion Database (T-NSMD)	754	1674	Akkar *et al.* (2010), Sandıkkaya *et al.* (2010)

*The data used within this study were selected by Cauzzi and Faccioli (2008).
†The data used within this study were selected by Pousse *et al.* (2005).

closest distance to the surface projection of the rupture plane. The focal depths of the events are less than 30 km and events that lack style-of-faulting (SoF) information were discarded. See Ⓔ Table S1 (available as an electronic supplement to this article) for lists of the magnitude, depth, SoF, V_{S30} and country-based variation of the database in terms of number of events, records, and stations.

Table 2 shows the types of *in situ* measurement techniques applied for the computation of V_S profiles at the strong-motion sites. The table also gives information about the exploration depth (maximum depth at which the final V_S measurement is computed) for the *in situ* measurements. The *in situ* measurement techniques of ~22% of the stations are not reported in the database. These stations are almost exclusively from the NGA database and their V_{S30} values reported by NGA project was considered as reliable in this article. The remaining stations that lack *in situ* measurement information are from the European Strong Motion Database (ESMD; Ambraseys, Douglas, *et al.*, 2004) and Internet Site for European Strong-motion Data (ISESD; Ambraseys, Smit, *et al.*, 2004) databases that are also known as well-documented strong-motion data sources. The V_{S30} values of sites for which the *S*-wave profiles do not reach to 30 m (i.e., profiles for which the exploration depths are less than 30 m) were computed by extending the *S*-wave velocity of the last layer to 30 m. This method is proposed by Boore (2004) and it yields, though relatively safer, comparable V_{S30} values with those of soil columns that have a complete V_S profile down to 30 m.

Table 2
Types of Measurements That Applied to Compute the *S*-Wave Velocity Profiles of the Sites Used in this Article. Exploration Depth Information is Also included in the Table

In situ Measurement*	Exploration Depth < 30 m	Exploration Depth > 30 m	Unknown
Crosshole	1	24	—
Downhole	515	552	—
MASW	—	139	—
SASW	3	4	—
SLT	5	17	—
Others	1	13	—
Unknown	2	260	96

*MASW, Multi-channel analysis of surface waves; SASW, spectral analysis of surface waves analysis; SLT, Suspension logging test

Figure 3 shows various distribution plots about the strong-motion database of this article. Figure 3a displays the M_w versus R_{JB} scatters of the entire database, whereas Figure 3b shows the M_w versus R_{JB} distribution of the subset of the database (records having $V_{S30} \geq 550$ m/s) that is used in the derivation of the reference-rock GMPE (see details in Proposed Site Model). The M_w versus R_{JB} plots that are given for the entire database and its subset (Fig. 3a,b, respectively) indicate a sparse data distribution for large-distance ($R_{JB} > 100$ km) and small-magnitude records. The distance-dependent distribution of the entire database (Fig. 3a) is fairly uniform for $5 \leq M_w \leq 7$. This uniform distribution gradually diminishes towards larger magnitudes ($M_w > 7$). Inherently, the M_w versus R_{JB} distribution of the subset is poorer with respect to the one given for the entire database as we constrained the data for records having soft-to-hard rock conditions (i.e., $V_{S30} \geq 550$ m/s). Figure 3c shows V_{S30}-dependent PGA variation of the entire database. Records that are on the right side of the solid black line (i.e., records having $V_{S30} \geq 550$ m/s) are used in the derivation of reference-rock ground-motion model. As one can infer from the distribution given in Figure 3c, the bulk of the data are within 200 m/s $\leq V_{S30} \leq$ 700 m/s. The records having $0.002g \leq$ PGA $\leq 0.2g$ are uniformly distributed within this V_{S30} interval. Data outside of this V_{S30} range lose their homogeneity in particular for $V_{S30} > 1000$ m/s and for large PGA values (PGA $\geq 0.1g$). Loose data distribution for hard-rock conditions is frequently observed in empirical strong-motion databases (e.g., NGA strong-motion database). Nonuniform data distribution of large PGA values is due to the sparse large-magnitude and short-distance recordings in our database at both ends of the V_{S30} limits considered in this article. Although the database used in this article is compiled from a considerably large strong-motion databank (SHARE SMdatabank), its aforementioned limitations (due to imposed constraints as explained

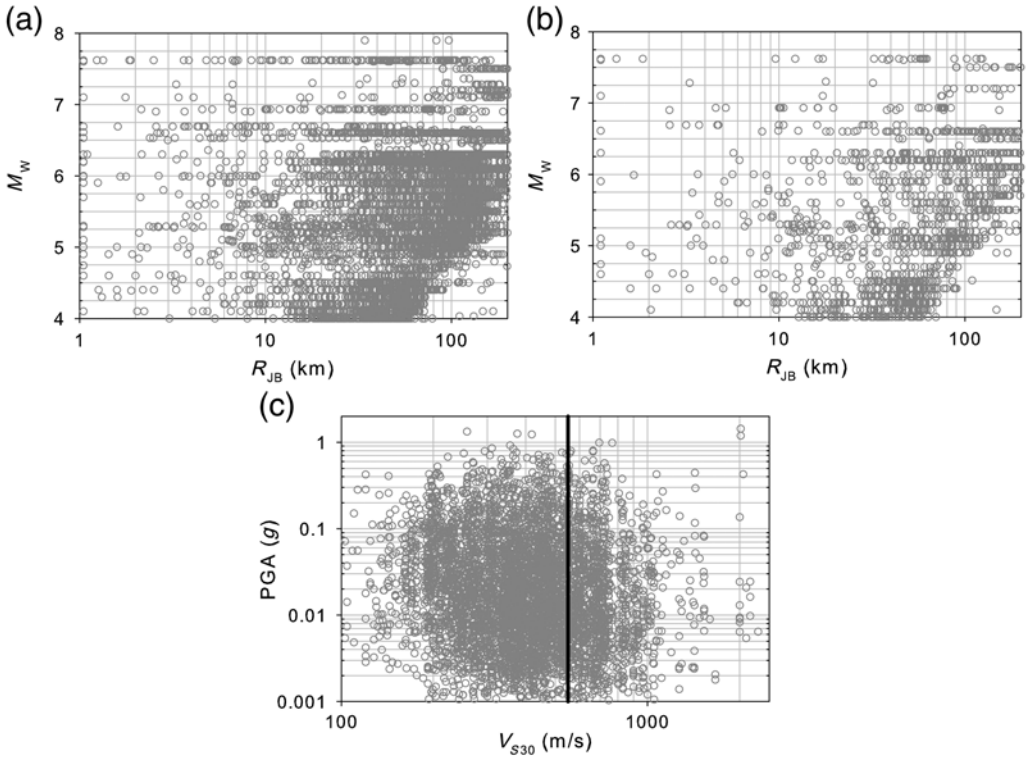

Figure 3 (a) R_{JB} versus M_w scatters of the entire database used in the derivation of site-amplification model, (b) subset of (a) used in the derivation of PGA_{REF} GMPE, (c) PGA versus V_{S30} scatters of the entire database. The solid black line in (c) separates the data at $V_{S30} = 550$ m/s.

throughout this section) will certainly confine the findings of this article. However, as discussed in the following sections, our results are generally consistent with the expected behavior of site amplification. The observed differences with other similar-type models arise from the modeling approach and different features of the datasets used in each study.

Proposed Site Model

The model presented here favors the functional form proposed by WAS08 because it is relatively simple compared with other models. The WAS08 model is calibrated by considering (a) the limitations of our database, (b) the interpretations made on the observed amplification trends that were discussed previously (Figs. 1 and 2), and (c) the residual trends of the regression analyses that will be discussed in this section. The following paragraphs describe the steps and the methodology implemented to finalize the functional form of the site model.

We made a modification in WAS08 before starting the regression analysis. Instead of using a period-dependent reference velocity (V_{LIN}) as proposed by WAS08, a period-independent reference velocity (V_{REF}) is preferred (e.g., BA08 and CY08 site models) to simplify the proposed expression. This choice is based on our preliminary investigations about site-amplification models that use period-dependent reference velocity. In such models period-dependent reference velocity attains significantly small values as spectral ordinates shift towards longer periods (e.g., AS08 assumes a reference velocity of 400 m/s for $T \geq 1.0$ s), which cannot be justified by our database. Site models that use period-independent reference velocity (such as the one proposed in this article) would impose slightly higher nonlinearity with respect to those that consider period-dependent reference velocity. However, this difference is not significant as it will be shown in the following paragraphs. The use of V_{REF} also eliminates the need for the d term in WAS08 thus making the regression analysis simpler. The PGA_{1100} parameter in WAS08 (PGA_{REF} in our model) that describes the input rock motion is also used in our model, because changing it to reference-rock spectral-acceleration ordinates (as in the case of CY08) would complicate the model. In fact, our preliminary analyses did not show any improvements in the proposed site model by changing input rock PGA (PGA_{REF}) to input rock spectral acceleration.

In order to understand the capability of the strong-motion database in addressing the nonlinear site effects, a preliminary set of analyses was done by setting the nonlinear site terms to zero, that is, $b(T) = 0$. These analyses showed that the increase in the level of input rock motion results in reduced site-amplification factors indicating the existence of nonlinear behavior in soil sites. The residuals of this preliminary study also revealed relatively lower site-amplification estimations at high V_{S30} values. Thus, the site amplification was held fixed for higher V_{S30} values. This behavior is also

observed in AS08. The threshold limit for V_{S30} to fix the site amplification is referred to as V_{CON} in our model. Although the data are inadequate to determine the limiting shear-wave velocity, V_{CON} is constrained to 1000 m/s. The final functional form of the proposed model is given in equation (5)

$$\ln(\mathrm{Amp}) = \begin{cases} a(T)\ln(V_{S30}/V_{\mathrm{REF}}) + b(T)\ln\left[\frac{\mathrm{PGA}_{\mathrm{REF}} + c(V_{S30}/V_{\mathrm{REF}})^n}{(\mathrm{PGA}_{\mathrm{REF}} + c)(V_{S30}/V_{\mathrm{REF}})^n}\right] & \text{for } V_{S30} < V_{\mathrm{REF}} \\ a(T)\ln(V_{S30}/V_{\mathrm{REF}}) & \text{for } V_{\mathrm{REF}} \le V_{S30} < V_{\mathrm{CON}} \\ a(T)\ln(V_{\mathrm{CON}}/V_{\mathrm{REF}}) & \text{for } V_{S30} \ge V_{\mathrm{CON}} \end{cases} \quad (5)$$

for which $a(T)$, $b(T)$, c, and n are regression coefficients. The parameter, V_{REF}, is the period independent reference V_{S30} ($V_{\mathrm{REF}} = 750$ m/s as explained in the below paragraph). $\mathrm{PGA}_{\mathrm{REF}}$ (in g; gravitational acceleration) is the level of input rock motion at V_{REF}. It is estimated from the reference-rock ground-motion model (see following paragraph) that is developed from the dataset used in this article. The coefficient c provides the transition between higher and lower ground-motion amplitudes. The coefficient n mainly captures the soil nonlinearity at low V_{S30} sites.

The recordings from sites for which the $V_{S30} \ge 550$ m/s were selected as a subset of the entire database to derive the ground-motion model for estimating the reference-rock motion, $\mathrm{PGA}_{\mathrm{REF}}$. Figure 3b shows an M_{w} versus R_{JB} scatter plot of this dataset. This subset consists of 1355 recordings collected from 283 events and 344 strong-motion stations. The magnitude and distance ranges of the subset are $4 \le M_{\mathrm{w}} \le 7.6$ and $R_{\mathrm{JB}} \le 200$ km, respectively. The average V_{S30} of the recordings in the subset is 750 m/s that is considered to be the period-independent reference velocity (V_{REF}) in our model. A functional form similar to AS08 was used in the derivation of the $\mathrm{PGA}_{\mathrm{REF}}$ ground-motion model (equation 6). This functional form represents the overall trends in the subset fairly well:

$$\begin{aligned} &\text{for } M_{\mathrm{w}} \le 6.75; \ln(\mathrm{PGA}_{\mathrm{REF}}) \\ &= 3.17101 + 1.15371(M_{\mathrm{w}} - 6.75) \\ &\quad + 0.0803(8.5 - M_{\mathrm{w}})^2 + [-1.49513 \\ &\quad + 0.13602(M_{\mathrm{w}} - 6.75)] \\ &\ln(\sqrt{R_{\mathrm{JB}}^2 + 13.39544^2} - 0.35736F_{\mathrm{N}} + 0.06573F_{\mathrm{R}} \\ &\text{for } M_{\mathrm{w}} > 6.75; \ln(\mathrm{PGA}_{\mathrm{REF}}) \\ &= 3.17101 - 0.31204(M_{\mathrm{w}} - 6.75) \\ &\quad + 0.0803(8.5 - M_{\mathrm{w}})^2 + [-1.49513 \\ &\quad + 0.13602(M_{\mathrm{w}} - 6.75)] \\ &\ln(\sqrt{R_{\mathrm{JB}}^2 + 13.39544^2} - 0.35736F_{\mathrm{N}} + 0.06573F_{\mathrm{R}}. \end{aligned} \quad (6)$$

In equation (6) the multiplier of the logarithmic distance term accounts for the magnitude-dependent ground-motion decay. It also controls the saturation of high-frequency ground motions at short distances (AS97). The functional form includes quadratic magnitude term with a break in linear magnitude scaling. The parameters F_{N} and F_{R} are dummy variables for the influence of style-of-faulting, taking values of one for normal and reverse faults, respectively, and zero otherwise. Our functional form for $\mathrm{PGA}_{\mathrm{REF}}$ estimations does not contain an independent parameter to account for the depth-to-rock effect on $\mathrm{PGA}_{\mathrm{REF}}$ amplitudes that is either defined as $Z1.0$ or $Z2.5$ in most of the NGA GMPEs. Such information is very limited in our subset for its inclusion as an estimator parameter. The reference-rock model coefficients were obtained from the random-effects regression analysis (Abrahamson and Youngs, 1992) for the geometric mean of two horizontal components.

Figure 4 compares the derived reference-rock ground-motion model with the three NGA GMPEs for $V_{S30} = 750$ m/s. Although the subset used for the reference-rock model is limited due to sparsely distributed high-V_{S30} data (for example there are only 113 records for $\mathrm{PGA} \ge 0.1g$ for $V_{S30} \ge 550$ m/s as given in Fig. 3c), the reference-rock estimations of our model are fairly comparable with the NGA GMPEs. This observation may suggest using one of the other NGA models for estimating $\mathrm{PGA}_{\mathrm{REF}}$. We did not prefer this option, because NGA GMPEs consider some particular estimator parameters (e.g., $Z1.0$, $Z2.5$, R_{X}, depth to top-of-rupture) that may be difficult to obtain in many cases unless particular assumptions are made for each earthquake scenario. (Some recent publications, such as Kaklamanos *et al.* [2011] suggest pragmatic approaches to compute the missing parameters in NGA GMPEs.) Moreover, these GMPEs are derived from the subsets of the NGA strong-motion databank (Power *et al.*, 2008), which may fail to reflect some of the specific features of the dataset used in the derivation of our $\mathrm{PGA}_{\mathrm{REF}}$ GMPE. We also wanted to have a complete set of tools while deriving our site model in order to verify one of the major objectives of this article: the validity of the WAS08 approach using observed data as well as give a full perspective on the modeling uncertainties associated with every stage in our article. In brief, the rock ground-motion model derived in this article yields slightly lower estimations with respect to other GMPEs for small magnitude events ($M_{\mathrm{w}} = 5.5$). The reference-rock estimations by our GMPE tend to be larger in the short-to-intermediate distance range for moderate (M_{w} 6.5) and large (M_{w} 7.5) magnitude events. The last observation may result in slightly higher soil nonlinearity in our site-amplification model.

Although it is not shown in this article, we also studied the distance-dependent behavior of within-event residuals of our reference-rock GMPE against different regions existing

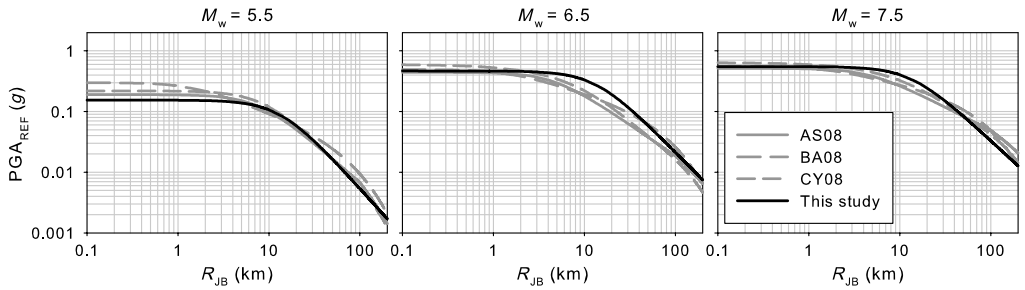

Figure 4 Comparison of the proposed rock estimations with three NGA GMPEs (AS08, BA08, and CY08) at $V_{S30} = 750$ m/s. The left, middle, and right column illustrate variation in M_w 5.5, M_w 6.5, M_w 7.5, respectively. The comparisons are done for a fictitious strike-slip fault with a dip angle of 90°, and the site is placed on the footwall side. The differences in the distance measures among the compared GMPEs were taken into account based on the simple scenario described here. Default values proposed by the model developers were used for some particular estimator parameters (e.g., $Z1.0$) that were employed in the NGA GMPEs.

in the dataset (pan-European region, Japan, and Taiwan, together with the U.S. records). The residual analysis did not map any regional dependency in particular at distances beyond 50 km where regional differences in geometric spreading may be dominant. Thus, we do not see any serious limitation to restrict the use of the reference-rock GMPE for source-to-site distances greater than 50 km. However, this observation should be considered with some reservation, because the reference-rock data are limited at long distances (only 506 recordings for $R_{JB} > 70$ km). Subdividing the limited data into different regions essentially decreases the size of each bin and this data-oriented limitation may cast some doubts about our conclusive remark on the insignificance of regional effects. Upon the increase in rock data with reliable V_{S30} information, we can improve our reference-rock GMPE by including additional estimator parameters to account for likely regional differences in the reference rock motion estimations.

The site-amplification factors, which are calculated by normalizing the observed spectral ordinates with the corresponding median estimations of the reference-rock motions at $V_{S30} = 750$ m/s, were used to obtain the site-model coefficients by applying the random-effects regression analysis. The coefficients c and n were only computed at $T = 0.0$ s and held fixed for the entire period range, because PGA_{REF} describes the input rock-motion level for nonlinear soil behavior in the proposed model. The site model is derived for 63 spectral-acceleration periods between $0.0 \text{ s} \le T \le 4.0$ s and for peak ground velocity (PGV). The regression coefficients and corresponding within- and between-event standard deviations (σ and τ, respectively) for a subset of the selected periods are given in Table 3 (see Ⓔ Table S2 in the supplement for the entire set of regression coefficients as well as the between- and within-event standard deviations). As can be inferred from Table 3, the $b(T)$ coefficient that controls the nonlinear soil behavior decreases with increasing period up to $T = 0.3$ s. This coefficient tends to increase towards longer periods (i.e., $T > 0.3$ s) that show the gradual decrease in soil nonlinearity. A similar behavior is also observed in WAS08, which indicates that the nonlinear site behavior derived from the empirical data of this article is consistent with the stochastic simulations of the WAS08 model. The top row in Figure 5 shows the between-event residual scatters of the proposed model as a function of magnitude. The middle and bottom rows on the same figure display the within-event residual distributions with respect to R_{JB} and V_{S30}, respectively. Each column in Figure 5 shows the variation of residuals for $T = 0.0$ s, $T = 0.2$ s, and $T = 1.0$ s. The random variation of residual trends in these particular spectral periods would give an overall idea about the success of the proposed model. They advocate that the site amplifications estimated by the model are unbiased as the variations in residuals are random in terms of selected

Table 3
Regression Coefficients and Corresponding Standard Deviations for the Site-Amplification Model (The Constant Values for c, n, V_{CON}, and V_{REF} are Given in the Footnote)†

Period	a	b	σ*	τ*	σ_T*
PGA	−0.41997	−0.28846	0.6448	0.4981	0.8148
PGV	−0.72057	−0.19688	0.6828	0.6823	0.9653
0.01	−0.41729	−0.28685	0.6452	0.4984	0.8153
0.02	−0.39998	−0.28241	0.6459	0.5042	0.8194
0.03	−0.34799	−0.26842	0.6510	0.5146	0.8298
0.04	−0.27572	−0.24759	0.6580	0.5305	0.8452
0.05	−0.21231	−0.22385	0.6658	0.5432	0.8593
0.075	−0.14427	−0.17525	0.6968	0.5672	0.8985
0.1	−0.27064	−0.29293	0.7177	0.5745	0.9193
0.15	−0.48313	−0.39551	0.7158	0.5324	0.8921
0.2	−0.65315	−0.44644	0.7048	0.5076	0.8686
0.3	−0.82609	−0.45730	0.6874	0.4995	0.8497
0.4	−0.89517	−0.43008	0.6803	0.5017	0.8453
0.5	−0.94614	−0.37408	0.6650	0.4889	0.8254
0.75	−1.00786	−0.28957	0.6516	0.4749	0.8063
1	−1.01331	−0.28702	0.6574	0.4663	0.8060
1.5	−0.98071	−0.24695	0.6556	0.4778	0.8112
2	−0.91007	−0.17336	0.6465	0.4712	0.8000
3	−0.85793	−0.13336	0.6330	0.4614	0.7833
4	−0.75645	−0.07749	0.6407	0.4950	0.8096

*The within- and between-event sigmas are denoted as σ and τ, respectively, and σ_T is the total standard deviation.

†$c = 2.5g$, $n = 3.2$, $V_{CON} = 1000$ m/s, and $V_{REF} = 750$ m/s.

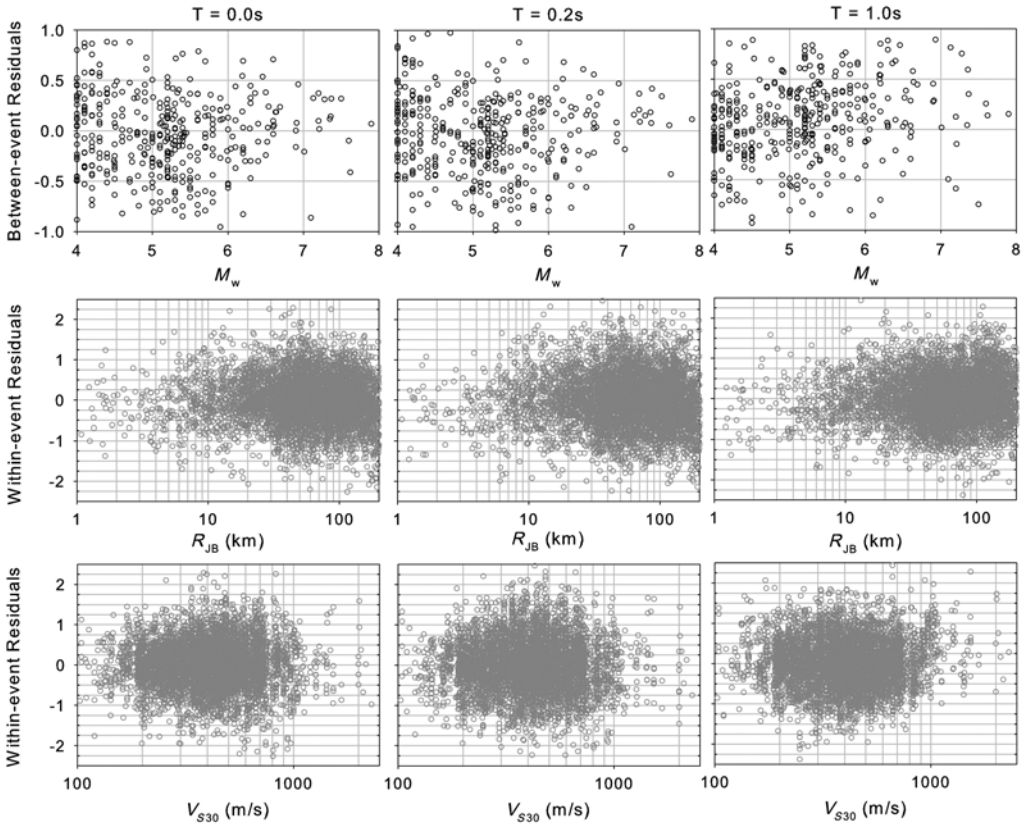

Figure 5 Between-event (top row) and within-event (other two rows) residual distribution of the proposed site model. Left, middle and right columns show the distribution for $T = 0.0$ s, $T = 0.2$ s, and $T = 1.0$ s, respectively.

seismological and geophysical parameters. Thus, its use would result in consistent site-amplification estimations for 150 m/s $< V_{S30} \leq$ 1200 m/s.

Evaluation of the Proposed Site Model

Figure 6 compares the proposed model (black solid line) with the variation of the data for different PGA_{REF} intervals. The comparisons are done for $T = 0.0$ s (first row) and spectral ordinates at $T = 0.2$ s and $T = 1.0$ s (middle and bottom row, respectively). For the first two periods, the nonlinear soil behavior is dominant. The nonlinearity in soil behavior starts diminishing significantly at $T = 1.0$ s, and almost vanishes for $T > 2.0$ s (not shown here). The figure also includes two of the NGA site models for comparison: AS08 (short dashed gray line) and BA08 (long dashed gray line). AS08 was modified to obtain amplification factors consistent with 750 m/s (i.e., V_{REF} in our model) because its reference PGA is defined at $V_{S30} = 1100$ m/s (PGA_{1100} in their terminology). The modification to AS08 is an iterative process: (a) assign an arbitrary PGA_{1100} value as an input for the AS08 site model, (b) compute site amplification SF from AS08 at $V_{S30} = 750$ m/s, (c) loop until the product of SF and PGA_{1100} equals target PGA_{REF} by modifying PGA_{1100} in each iteration, (d) when (c) is satisfied, the last SF is the calibrated site amplification of AS08 for the chosen PGA_{REF} and V_{REF} in our model.

The immediate observation from Figure 6 is that the estimated site amplifications of the proposed model are comparable with AS08 and BA08. This is expected because all models explicitly impose nonlinear soil behavior. On the other hand, each site-model plot in this figure shows its own characteristic features upon careful examination. This is also not strange, because the modeling approaches and the databases (including their metadata information) are different for each model, which result in such differences. These are discussed in the following paragraph.

When V_{S30} attains relatively large values ($V_{S30} \geq$ 1000 m/s) the site model presented in this article as well as AS08 cap the site amplification to a constant value to prevent very small amplification factors. All models seem to follow the data trend closely for 300 m/s $< V_{S30} \leq$ 1000 m/s. In other words, for increasing V_{S30} values, when soil behavior is presumably linear ($V_{S30} >$ 300 m/s), all models yield similar amplification factors. In general, for low V_{S30} values ($V_{S30} \leq$ 300 m/s), the site amplifications of the proposed model are slightly lower than those of AS08 and BA08. The observed differences between our model and other models indicate that the proposed site-amplification function imposes slightly higher nonlinearity for $PGA_{REF} < 0.2g$ for high-frequency ground motions (represented by $T = 0.0$ s and $T = 0.2$ s in Fig. 6), which might be due to the conservative PGA_{REF} estimations. Other factors, such as the

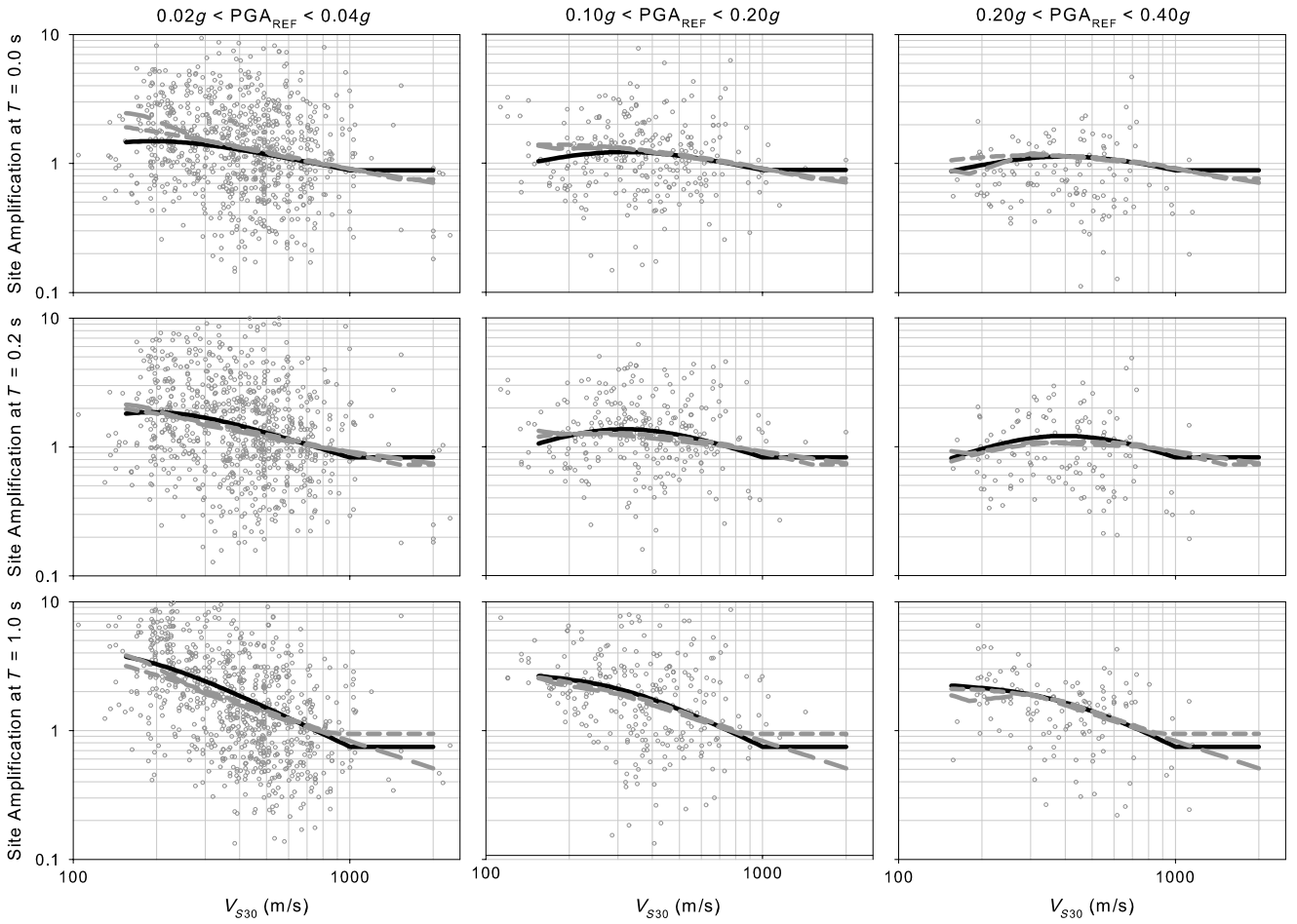

Figure 6 Comparisons of the proposed site model (black solid line) with AS08 (short-dashed gray curve) and BA08 (long-dashed gray curve) together with the empirical data for $T = 0.0$ s, $T = 0.2$ s, and $T = 1.0$ s (from top to bottom respectively). Each column represents different level of input rock motion, PGA_{REF} indicated at the top of figure.

ground-motion databases and functional forms, can also play role in the observed differences. The proposed site model is derived using the data points given in these figures, so relatively better agreement between the data and the estimations of the model should be expected. Another source of discrepancy between the data and the two NGA models could be their lower V_{S30} limits. The lowest V_{S30} value for these models is approximately 180 m/s, which is slightly higher than the minimum V_{S30} value given in these plots.

The above discussions suggest that soil nonlinearity is significant for high-frequency spectral ordinates (PGA or spectral acceleration at $T = 0.2$ s). This observation is particularly valid for the proposed model due to its specific features as discussed in the above paragraphs. This observation may contradict the site-amplification factors in some of the well-known seismic-design codes, such as Eurocode 8 (CEN, 2004). Eurocode 8 proposes period-independent site-amplification factors for PGA, which are greater than unity even for high PGA values. These recommendations are significantly different than the soil amplification behavior presented in this article. To test the reliability of our site model for code implementation the results of a comparative case study are presented in a tabular format in Table 4. The case study compares our site-amplification factors with those proposed in the updated NEHRP provisions (BSSC, 2009a). The NEHRP provisions consider nonlinear soil behavior as a function of five different spectral-acceleration levels at $T = 0.2$ s and $T = 1.0$ s. The reference rock is described by $V_{S30} = 760$ m/s in the NEHRP provisions, which is slightly higher than the one in our model (i.e., $V_{S30} = 750$ m/s). This difference is neglected in this article. The site-amplification comparisons are done for three site classes: NEHRP C (760 m/s $< V_{S30} \leq 360$ m/s), NEHRP D (360 m/s $< V_{S30} \leq 180$ m/s), and NEHRP E ($V_{S30} < 180$ m/s). We assumed that the geometric means of the upper and lower bound V_{S30} values can represent the NEHRP C and D site classes (i.e., $V_{S30} = 525$ m/s and $V_{S30} = 255$ m/s, respectively) in estimating the site amplifications from our model. NEHRP E site class was represented by $V_{S30} = 180$ m/s. Because the NEHRP provisions consider period-dependent site amplifications (for discrete spectral accelerations at $T = 0.2$ s and $T = 1.0$ s as presented in Table 4), we first computed the corresponding PGA_{REF} value for each discrete spectral-acceleration value for our site model. This is achieved by computing the

Table 4
Comparative Table that Lists the Recommended NEHRP Site Amplifications (First Numbers) and Corresponding Estimations (in Bold) from the Proposed Site Model

	Site Amplifications for Spectral Accelerations S_S at $T = 0.2$ s				
Site Class	$S_S = 0.25g$	$S_S = 0.50g$	$S_S = 0.75g$	$S_S = 1.00g$	$S_S = 1.25g$
C	1.20/**1.21**	1.20/**1.17**	1.10/**1.14**	1.00/**1.12**	1.00/**1.10**
D	1.60/**1.37**	1.40/**1.13**	1.20/**1.01**	1.10/**0.94**	1.00/**0.89**
E	2.50/**1.20**	1.70/**0.94**	1.20/**0.82**	0.90/**0.75**	0.90/**0.70**
	Site Amplifications for Spectral Accelerations at $T = 1.0$ s				
Site Class	$S_1 = 0.10g$	$S_1 = 0.20g$	$S_1 = 0.30g$	$S_1 = 0.40g$	$S_1 = 0.50g$
C	1.70/**1.39**	1.60/**1.34**	1.50/**1.32**	1.40/**1.31**	1.30/—
D	2.40/**2.22**	2.00/**1.88**	1.80/**1.81**	1.60/**1.74**	1.50/—
E	3.50/**2.48**	3.20/**2.00**	2.80/**1.92**	2.40/**1.85**	2.40/—

reference-rock regression coefficients (equation 6) for spectral-acceleration ordinates at $T = 0.2$ s and $T = 1.0$ s. These particular equations were used to identify the most appropriate earthquake scenario that would give approximately the same spectral-acceleration values indicated in the NEHRP provisions. The determined earthquake scenarios were then used in equation (6) to compute corresponding values of PGA_{REF}, which were, in turn, inserted into equation (5) to compute our site-amplification estimations. For each specific case, our site amplifications and those of NEHRP provisions are given side by side in Table 4. In order to distinguish our site-amplification estimations, they are given in boldface. Although we applied various intermediate steps to obtain the comparative site-amplification values from our model, they are fairly in good agreement with those recommended by the NEHRP provisions. The good agreement presented in Table 4 advocates the consistency of our site model in addressing the nonlinear soil behavior. It also emphasizes the importance of period dependency in site amplification for different reference-rock ground-motion intensity levels, as site factors are not the same for every case.

Figure 7 discusses the last remark in the above paragraph in a more detailed way. This figure shows period-dependent site amplifications of our model as well as those of AS08 and BA08 for three different V_{S30} values: $V_{S30} = 525$ m/s, $V_{S30} = 255$ m/s, and $V_{S30} = 180$ m/s. These values grossly represent the NEHRP C, D, and E site classes (as discussed in the above paragraph). They also characterize

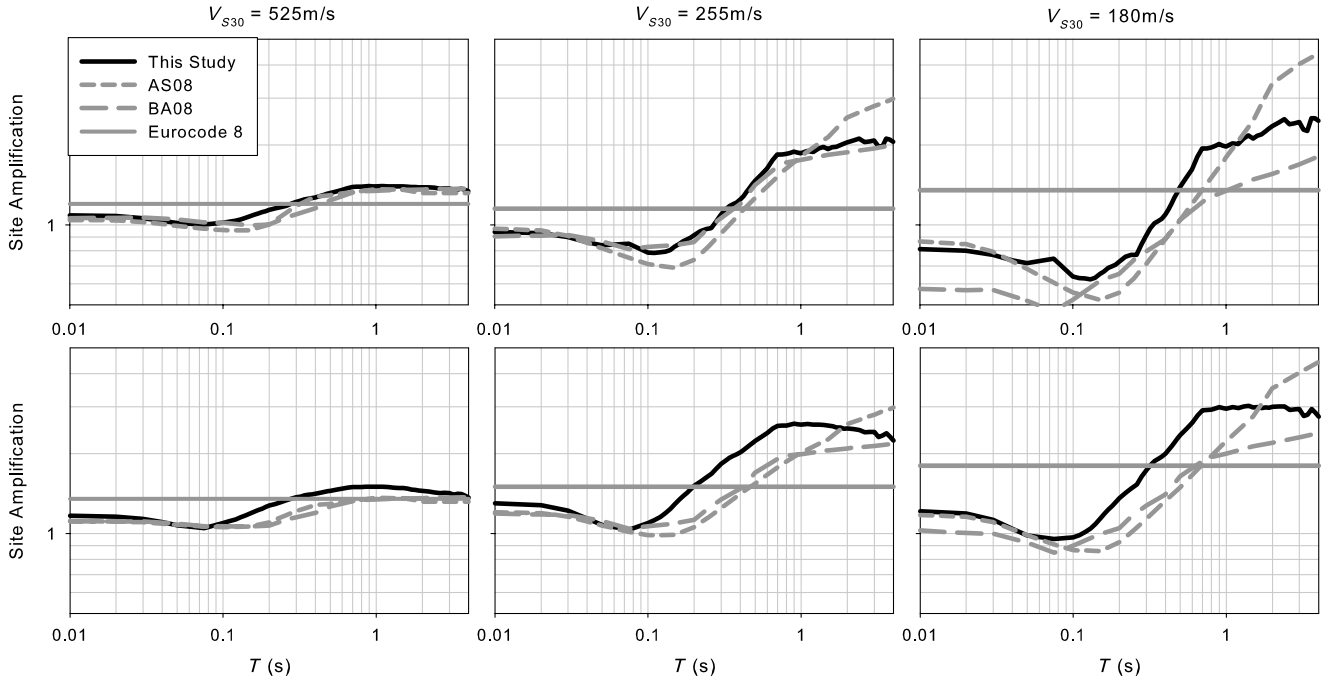

Figure 7 Period-dependent variation of site amplifications computed from the proposed model as well as AS08 and BA08 for high seismicity (M_w 7.5; top row) and low seismicity (M_w 5; bottom row) earthquake scenarios. The chosen V_{S30} values for site amplification calculations represent Eurocode 8 site classes B, C, and D that are comparable with the NEHRP C, D, and E site classifications, respectively. The plots contain Eurocode 8 site amplifications for the described earthquake scenarios that are designated as Type I (top row) and Type II (bottom row) in Eurocode 8.

the Eurocode 8 (CEN, 2004) B, C, and D site classes fairly well as their V_{S30} intervals are almost identical to those of NEHRP C, D, and E, respectively. The site amplifications were computed for two reference-earthquake scenarios that represent Type-I and Type-II hazard levels in Eurocode 8. The top row plots in Figure 7 show the amplifications calculated for a strike-slip earthquake scenario of M_w 7.5 (Type-I hazard level), whereas the bottom row panels give amplifications for an M_w 5 strike-slip event. For both cases the site is assumed to be located at a distance of $R_{JB} = 0.1$ km. The rock site condition used for computing site amplifications is mimicked by $V_{S30} = 800$ m/s, which is consistent with the Eurocode 8 rock definition. The panels on this figure also display the period-independent site factors of Eurocode 8 for Type-I (top row) and Type-II (bottom row) hazard levels.

The preliminary observation from these comparative plots is the fairly good match between the proposed model and the other two site models for $V_{S30} = 525$ m/s and $V_{S30} = 255$ m/s. The dispersive behavior of the three models becomes quite visible for soft soil ($V_{S30} = 180$ m/s) conditions, which may stem from the sparse low V_{S30} recordings in the ground-motion databases as well as the differences in the implemented modeling approach in each functional form. Nevertheless, even for soft soil conditions, the site-amplification trends imposed by these models are similar (the amplification estimations of our model as well as that of BA08 impose lower gradients for this site class as the vibration period increases). The other important observation from Figure 7 is the incompatible variation of period-independent site-amplification factors of Eurocode 8 with respect to other site models. The site amplifications suggested by Eurocode 8 are generally conservative in the short periods and they seem to fail following the trends of other site models towards longer periods. We note that this observation is limited to the selected earthquake scenario and it should be validated further by a comprehensive study.

Conclusions

This article presents an empirical site-amplification model that can be used in GMPEs derived for shallow active crustal regions. The functional form is capable of addressing the linear and nonlinear soil behavior and it is based on a well-studied extensive dataset with the most recent updates of the Greek, Italian, and Turkish site information. Therefore, it can be of particular use for future pan-European GMPEs. A ground-motion predictive model is also derived to estimate the level of input rock motion (PGA_{REF}) that is used in the calculation of site-amplification factors. The reference-rock motion is defined as $V_{S30} = 750$ m/s in our article. Confined to the limitations of the strong-motion database, we recommend the use of our site model for 150 m/s $< V_{S30} <$ 1200 m/s.

The functional form of the proposed site model carries similar features with the one in WAS08 that is entirely based on stochastic simulations. The consistency of our site amplifications with those of the WAS08 model validates the theoretical aspects of WAS08 through the use of empirical data. The agreement between these comparisons also advocates the reliability and robustness of our site model. Notwithstanding, the proposed model also draws consistent trends with other similar site-amplification equations (e.g., BA08). It imposes slightly higher soil nonlinearity for softer sites due to differences in modeling approach, strong ground-motion database, and PGA_{REF} GMPE. The observed trends in the proposed site model are also consistent with the NEHRP seismic provisions that consider period-dependent nonlinear soil behavior. The preliminary discussions presented here can also be taken into account by Eurocode 8 committees for future modifications in site-amplification factors that are currently independent of soil nonlinear behavior as well as vibration period.

Data and Resources

The ground motions and corresponding metadata used in this article are gathered and re-evaluated from the Turkish (http://kyh.deprem.gov.tr/ftpt.htm, last accessed September 2009), Italian (http://itaca.mi.ingv.it/ItacaNet, last accessed July 2011), NGA (http://peer.berkeley.edu/peer_ground_motion_database, last accessed September 2009), European (http://www.isesd.hi.is/ESD_Local/frameset.htm, last accessed November 2009) and Japanese (http://www.kik.bosai.go.jp, last accessed June 2011 and http://www.k-net.bosai.go.jp, last accessed June 2011) databases. Some of the shear-velocity profiles are downloaded from both the personal webpage of D. M. Boore (www.daveboore.com, last accessed June 2011) and the Rosrine Project website (Nigbor *et al.*, 2001).

Acknowledgments

The main part of this work has been funded by the EC-Research Framework programme FP7, Seismic Hazard Harmonization in Europe (SHARE), Contract Number 226967. We also thank the Associate Editor, John Douglas, and two anonymous reviewers for their comments for improving the quality of the article.

References

Abrahamson, N. A., and W. J. Silva (1997). Empirical response spectral attenuation relations for shallow crustal earthquakes, *Seismol. Res. Lett.* **68,** 94–127.

Abrahamson, N. A., and W. Silva (2008). Summary of the Abrahamson and Silva NGA ground motion relations, *Earthq. Spectra* **24,** 67–98.

Abrahamson, N. A., and R. R. Youngs (1992). A stable algorithm for regression analyses using the random effects model, *Bull. Seismol. Soc. Am.* **82,** 505–510.

Akkar, S., and J. J Bommer (2010). Empirical equations for the prediction of PGA, PGV and spectral accelerations in Europe, the Mediterranean region and the Middle East, *Seismol. Res. Lett.* **81,** 195–206.

Akkar, S., Z. Çağnan, E. Yenier, Ö. Erdoğan, M. A. Sandıkkaya, and P. Gülkan (2010). The recently compiled Turkish strong-motion database: Preliminary investigation for seismological parameters, *J. Seismol.* **14,** 457–479.

Ambraseys, N. N., J. Douglas, R. Sigbjörnsson, C. Berge-Thierry, P. Suhadolc, G. Costa, and P. Smit (2004). *Dissemination of European*

Strong Motion Data Using Strong Motion Datascape Navigator, Vol. 2, CD-ROM collection, Engineering and Physical Sciences Research Council, United Kingdom.

Ambraseys, N. N., P. Smit, J. Douglas, B. Margaris, R. Sigbjörnsson, S. Olafsson, P. Suhadolc, and G. Costa (2004). Internet site for European strong-motion data, *Boll. Geofis. Teor. Appl.* **45,** 113–129.

Boore, D. M. (2004). Estimating $V_S(30)$ (or NEHRP Site Classes) from shallow velocity models (depths < 30 m), *Bull. Seismol. Soc. Am.* **94,** 591–597.

Boore, D. M. (2005). SMSIM—Fortran Programs for Simulating Ground Motions from Earthquakes: Version 2.3—A Revision of OFR 96-80-A, *U.S. Geol. Surv. Open-File Rept.* (A modified version of OFR 00—509, describing the program as of 15 August 2005), Menlo Park, California.

Boore, D. M., and G. M. Atkinson (2008). Ground-motion prediction equations for the average horizontal component of PGA, PGV, and 5%-damped PSA at spectral periods between 0.01 s and 10.0 s, *Earthq. Spectra* **24,** 99–138.

Boore, D. M., and W. B. Joyner (1997). Site amplifications for generic rock sites, *Bull. Seismol. Soc. Am.* **87,** 327–341.

Boore, D. M., W. B. Joyner, and T. E. Fumal (1997). Equations for estimating horizontal response spectra and peak acceleration from western North American earthquakes: A summary of recent work, *Seismol. Res. Lett.* **68,** 128–153.

Borcherdt, R. D. (1970). Effects of local geology on ground motion near San Francisco Bay, *Bull. Seismol. Soc. Am.* **60,** 29–61.

Borcherdt, R. D. (1994). Estimates of site dependent response spectra for design (methodology and justification), *Earthq. Spectra* **10,** 617–653.

Borcherdt, R. D. (2002a). Empirical evidence for acceleration-dependent amplification factors, *Bull. Seismol. Soc. Am.* **92,** 761–782.

Borcherdt, R. D. (2002b), Empirical evidence for site coefficients in building-code provisions, *Earthq. Spectra* **18,** 189–218.

Building Seismic Safety Council (BSSC) (2009a). *2009 NEHRP Recommended Seismic Provisions For New Buildings and Other Structures: Part 1*, Provisions, Federal Emergency Management Agency (P-750), Washington, D.C.

Building Seismic Safety Council (BSSC) (2009b). *2009 NEHRP Recommended Seismic Provisions For New Buildings and Other Structures: Part 2*, Commentary to ASCE/SEI 7-, Federal Emergency Management Agency (P-750), Washington, D.C.

Campbell, K. W., and Y. Bozorgnia (2008). NGA ground motion model for the geometric mean horizontal component of PGA, PGV, PGD and 5% damped linear elastic response spectra for periods ranging from 0.01 to 10 s, *Earthq. Spectra* **24,** 139–171.

Cauzzi, C., and E. Faccioli (2008). Broadband (0.05 to 20 s) prediction of displacement response spectra based on worldwide digital records, *J. Seismol.* **12,** 453–475.

Chiou, B. S.-J., and R. Youngs (2008). An NGA model for the average horizontal component of peak ground motion and response spectra, *Earthq. Spectra* **24,** 173–215.

Chiou, B., R. Darragh, N. Gregor, and W. Silva (2008). NGA project strong-motion database, *Earthq. Spectra* **24,** 23–44.

Choi, Y., and J. P. Stewart (2005). Nonlinear site amplification as function of 30 m shear wave velocity, *Earthq. Spectra* **21,** 1–30.

Crouse, C. B., and J. W. McGuire (1996). Site response studies for purpose of revising NEHRP seismic provisions, *Earthq. Spectra* **12,** 407–439.

Dobry, R., R. D. Borcherdt, C. B. Crouse, I. M. Idriss, W. B. Joyner, G. R. Martin, M. S. Power, E. E. Rinne, and R. B. Seed (2000). New site coefficients and site classification system used in recent building seismic code provisions, *Earthq. Spectra* **16,** 41–67.

European Committee for Standardization (CEN) (2004). *Eurocode 8: Design of Structures for Earthquake Resistance—Part 1: General Rules, Seismic Actions and Rules for Buildings*, European Committee for Standardization, Brussels.

Field, E. H. (2000). A modified ground-motion attenuation relationship for southern California that accounts for detailed site classification and a basin-depth effect, *Bull. Seismol. Soc. Am.* **90,** S209–S221.

Kaklamanos, J., L. G. Baise, and D. M. Boore (2011). Estimating unknown input parameters when implementing the NGA ground-motion prediction equations in engineering practice, *Earthq Spectra* **27,** 1219–1235.

Lee, Y., and J. G. Anderson (2000). Potential for improving ground-motion relations in southern California by incorporating various site parameters, *Bull. Seismol. Soc. Am.* **90,** S170–S186.

Luzi, L., S. Hailemikael, D. Bindi, F. Pacor, F. Mele, and F. Sabetta (2008). ITACA (ITalian ACcelerometric Archive): A web portal for the dissemination of the Italian strong motion data, *Seismol. Res. Lett.* **79,** 716–722.

Ni, S.-D., J. G. Anderson, Y. Zeng, and R. V. Siddharthan (2000). Expected signature of nonlinearity on regression for strong ground-motion parameters, *Bull. Seismol. Soc. Am.* **90,** S53–S64.

Nigbor, R. L., J. Diehl, and J. Swift (2001). Characterization of US Sites: ROSRINE 5B, PEER Lifelines Research Project 2A01—Site Response, Presented at *2001 PEER Annual Meeting*, 25–26 January Oakland, California.

Pousse, G., C. B. Thierry, and P.-Y. Bard (2005). Eurocode 8 design response spectra evaluation using the K-NET Japanese database, *J. Earthq. Eng.* **9,** 547–574.

Power, M., B. Chiou, N. Abrahamson, Y. Bozorgnia, T. Shantz, and C. Roblee (2008). An overview of the NGA project, *Earthq. Spectra* **24,** 3–21.

Rodriguez-Marek, A., J. D. Bray, and N. A. Abrahamson (2001). An empirical geotechnical seismic site response procedure, *Earthq. Spectra* **17,** 65–87.

Sadigh, K., C. Y. Chang, J. A. Egan, F. Makdisi, and R. R. Youngs (1997). Attenuation relationships for shallow crustal earthquakes based on California strong motion data, *Seismol. Res. Lett.* **68,** 180–189.

Sandıkkaya, M. A., M. T. Yılmaz, B. S. Bakır, and Ö. Yılmaz (2010). Site classification of Turkish national strong-motion stations, *J. Seismol.* **14,** 543–563.

Sokolov, V. Y. (1997). Empirical models for estimating Fourier-amplitude spectra of ground acceleration in the northern Caucasus (Racha seismogenic zone), *Bull. Seismol. Soc. Am.* **87,** 1401–1412.

Sokolov, V. Y. (2000). Hazard-consistent ground motions: Generation on the basis of uniform hazard Fourier spectra, *Bull. Seismol. Soc. Am.* **90,** 1010–1027.

Steidl, J. H. (2000). Site response in southern California for probabilistic seismic hazard analysis, *Bull. Seismol. Soc. Am.* **90,** S149–S169.

Stewart, J. P., A. H. Liu, and Y. Choi (2003). Amplification factors for spectral acceleration in tectonically active regions, *Bull. Seismol. Soc. Am.* **93,** 332–352.

Thompson, E. M., L. G. Baise, R. E. Kayen, E. C. Morgan, and J. Kaklamanos (2011). Multiscale site response mapping: A case study of Parkfield, California, *Bull. Seismol. Soc. Am.* **101,** 1081–1100.

Walling, M., W. Silva, and N. A. Abrahamson (2008). Nonlinear site amplification factors for constraining the NGA models, *Earthq. Spectra* **24,** 243–255.

Yenier, E., M. A. Sandıkkaya, and S. Akkar (2010). Report on the fundamental features of the extended strong-motion databank prepared for the SHARE Project, *Workshop for WP4*, Ankara, Turkey.

Earthquake Engineering Research Center
Middle East Technical University
06800 Ankara, Turkey
askaya@metu.edu.tr
sakkar@metu.edu.tr
(M.A.S., S.A.)

ISTerre (Institut des Sciences de la Terre)
Universite de Grenoble
38041 Grenoble Cedex 9, France
pierre-yves.bard@obs.ujf-grenoble.fr
(P.-Y.B.)

Manuscript received 6 January 2012